Journal of Alloys and Compounds 509 (2011) 3644–3650

Contents lists available at ScienceDirect

Journal of Alloys and Compounds

journal homepage: www.elsevier.com/locate/jallcom

Synthesis and characterization of spray deposited PdO–NiO–SDC composite anode material for potential application in IT-SOFC

B.B. Patil[a,*], S.H. Pawar[b]

[a] Department of Chemical Engineering, I.I.T. Delhi, New Delhi 110016, India
[b] D.Y.Patil University, Kasaba Bawada, Kolhapur 416 006, (M.S), India

ARTICLE INFO

Article history:
Received 22 November 2010
Received in revised form
16 December 2010
Accepted 17 December 2010
Available online 23 December 2010

Keywords:
Fuel cell
Chemical synthesis
Electronic properties
Atomic force microscopy (AFM)
X-ray diffraction

ABSTRACT

The synthesis of mixed conducting PdO–NiO–SDC composite films has been reported for the first time by a simple and cost effective spray pyrolysis technique. The films were deposited at low substrate and annealing temperatures of 350 °C and 500 °C, respectively. The structure, morphology and electrical properties of the films were studied by X-ray diffraction (XRD), scanning electron microscope (SEM), energy dispersive X-ray analysis (EDAX), atomic force microscopy (AFM) and impedance spectroscopy (IS). The substrate and annealing temperatures were optimized for obtaining nano-crystalline, porous, adherent and composite films with PdO, NiO and SDC phases. Films showed good microstructure with sufficient porosity and good connectivity of the deposited material. Crystallite size of the deposited material was found to be in the range of 7–9 nm. The deposited film showed high oxygen ion conductivity, 3.94×10^{-1} S cm^{-1} at 350 °C. Due to their nano-crystalline, porous and composite nature the spray deposited PdO–NiO–SDC films may have high three phase boundary area and hence can be considered as an anode for intermediate temperature solid oxide fuel cells.

1. Introduction

One of the key technological challenges the solid oxide fuel cell (SOFC) technology facing is the cost reduction. The success to the cost reduction depends critically on the development of novel electrodes for low temperature operations. The function of fuel cell critically depends on electrodes/electro-catalysts. Within the electrodes, the electrochemical reaction can only occur at the three phase boundary i.e. the point at which gas, ions and electrons meet. If there is a break down in any one of the three phases, the reaction cannot occur. Hence, electrode microstructure must provide as much as possible three phase boundary area.

In SOFC, electrodes must be porous, electronically and ionically conducting, electrochemically active, and have high surface area for catalytic action. It is rare for a single material to meet all these requirements, especially at low temperatures. Hence a composite electrode, of which the electro-catalyst is one component, is often utilized. Composites having porous and mixed ionic and electronic conductors (MIECs) have been widely used as electrodes to extend reaction site from the three phase boundaries to the surface of MIEC electrode.

Ni-YSZ cermet is most widely used anode material in solid oxide fuel cell systems [1,2]. Nickel (Ni) contains excellent properties regarding chemical, electrochemical, catalytical activity with a high electrical conductivity and is stable at high temperature during processing and operations [1]. Ni is a very good bond breaker of both the H–H and C–H bond in CH_4 [3]. Also, Ni is inexpensive and hence is most universally used as an anode in SOFC. However, major limitations of Ni-based anodes are that Ni catalyses the formation of graphitic carbon at low H_2O/C ratios [4]. Another problem with Ni is that it has low melting temperature. Hence, Ni is liable to agglomerate and change shape during consolidation and subsequent operation. A marked drop in electrical conductivity of anode cermet has been observed after being exposed to fuel gases for prolonged period of time, which is associated with the growth of the Ni particle size [5]. This drop in anode performance may be due to a reduction in both three phase boundary and electrical conductivity. However, no anode material is available that allows operation directly with hydrocarbons with a performance comparable to a Ni containing anode with hydrogen. Hence, there is necessity to reduce the carbon formation in the cell by modifying them. Instead of modifying Ni-YSZ cermet anodes investigations also performed on the use of electronic and mixed conducting oxides to make alternative metal/oxide cermets.

Ceria (CeO_2), a stable fluorite type oxide, is usually considered to provide mixed-electronic and ionic conductivity [6]. Among oxides, ceria is one of the better catalysts for total oxidation of hydrocarbons [7]. It has been shown that CeO_2 anode can electrochemically oxidize dry methane, as the presence of mobile lattice oxygen reduces the rate of carbon deposition [8,9]. Also, doped or un-doped

* Corresponding author. Tel.: +91 11 2659 6115; fax: +91 11 2685 1169.
E-mail address: bhartibpatil_2003@yahoo.co.in (B.B. Patil).

0925-8388/$ – see front matter © 2010 Elsevier B.V. All rights reserved.
doi:10.1016/j.jallcom.2010.12.134

ceria oxides are commonly applied as sulfur-tolerant components in metal cermet anodes due to good performance and low cost relatively to available alternatives [10–12].

Compared with CeO_2, doped ceria oxide exhibits approximately two orders of magnitude higher ionic conductivity due to extra oxygen vacancies introduced by doping with low valence ion [13] and maintain good stability against H_2S plus considerable catalytic activity for oxidizing H_2. Ni + doped ceria anodes with different Ni contents exhibit both higher performance with practical fuels and remarkable sulfur tolerance compared to the Ni-YSZ anodes. The enhanced performance is attributed to the enlargement of reactive sites [14–18].

Another material, NiO–samaria doped ceria (SDC), has been used as anodes for intermediate temperature solid oxide fuel cells [19–23]. In the present investigation SDC is added to Ni. The SDC constitutes the framework for the dispersion of Ni particles and acts as the inhibitor for the coarsening of Ni particles. Further, it offers a significant part of ionic conductivity, broadening effectively the three phase area [24]. High oxide conduction in doped ceria makes it possible to decrease SOFC operation temperature, thus reducing the numerous technological problems. Also, in fuel rich condition Ce^{4+} reduces to Ce^{3+} introducing electronic conductivity, and this property of ceria has been explored for the anode application [25]. Recently the influence of palladium addition to the NiO–SDC or NiO–GDC anodes on the cell performance has been studied and compared to an unmodified cell. It has been reported that Pd containing anode allow for higher power outputs [26–28]. This is due to the fact that metals (Pd, Pt, Rh) had much higher specific rates for water gas shift reaction, steam reforming and carbon dioxide reforming of methane when supported on ceria than when supported on silica or alumina [29,30]. Pd, Pt, Ru show far higher oxidation activity than ceria or any other oxide [31]. Thus, an addition of an oxidation catalyst such as Pd can promote complete oxidation of hydrocarbon and generate more heat to increase the cell temperature [26].

In the present investigation nano-crystalline, porous and adherent, mixed ionic and electronic conductor PdO–NiO–SDC composite thin films have been successfully deposited by a simple cost effective spray pyrolysis technique at low substrate and annealing temperature of 350 and 500 °C respectively. Deposited films have high oxygen ionic conductivity than that reported for the doped ceria films.

This material was earlier synthesized by different methods [26–28] and with best of our knowledge no work has been reported on deposition of this composite material by spray pyrolysis technique. In the present investigation spray synthesis and studies on structural, morphological and electrical properties of PdO–NiO–SDC films are reported for the first time.

2. Experimental

Precursor solution required to deposit 2 wt % PdO–NiO–SDC films, was prepared by dissolving stoichiometric amount of reagent grade palladium chloride ($PdCl_2$), nickel nitrate, $Ni(NO_3)_2{\cdot}6H_2O$, cerium (III) nitrate $Ce(NO_3)_3{\cdot}6H_2O$ and samarium nitrate, with $Ni:Ce_{0.8}Sm_{0.2}O_{1.9}$ as 7:3, in double distilled water. For this, samarium oxide (Sm_2O_3) was completely dissolved in nitric acid (HNO_3) to obtain corresponding nitrate. Concentration of the solution was kept as 0.1 M. The atomic ratio of cerium to samarium was set to 80:20 to give the highest ionic conductivity [32]. Ultrasonically cleaned plane glass plates were used as substrates. Optimized parameters for the deposition of good quality, adherent thin films were, spray rate – 1 ml/min, concentration of precursor solution – 0.1 M, quantity of solution – 40 ml. Substrate temperature of the films was varied from 300 to 450 °C with an interval of 50 °C. Films were then heat treated at 500 °C for 2 h in tubular furnace. These films were described as S300, S350, S400 and S450 respectively. The films were then characterized by X-ray diffraction (XRD) technique. Film thickness was calculated by using weight difference method by using the formula:

$$t = \frac{\text{weight difference}}{A\rho} \quad (1)$$

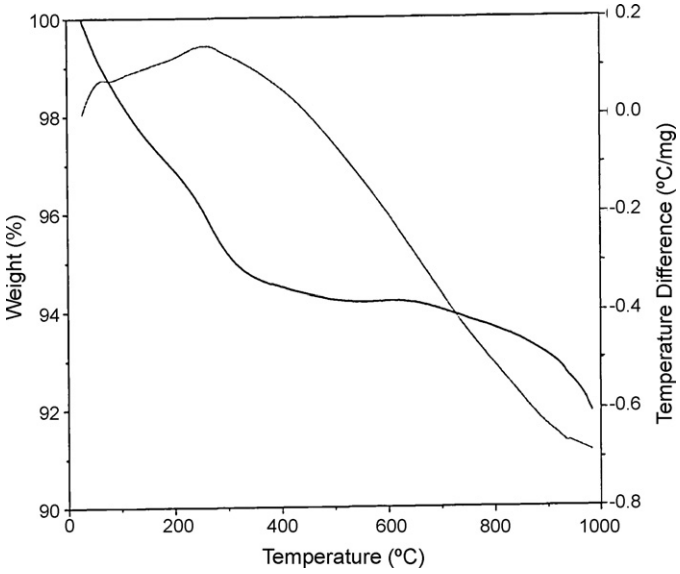

Fig. 1. The simultaneous DTA–TGA curves of spray deposited PdO–NiO–SDC powder.

where A is the area of the film and ρ is the density of the bulk material and density was taken as 6.94 g/cm^3.

The material from as deposited thin films was scratched out from the substrate and then differential thermal analysis (DTA) and thermogravimetric analysis (TGA) were studied by using an instrument SDT-2960, TA Inc., USA, with a heating rate 10 °C/min from 10 to 1000 °C in air environment. The films were characterized by X-ray diffraction (XRD) technique using Phillips PW-1710 diffractometer with CuK_α radiation having wavelength 1.5424 Å and scanning range of 10–100°. The crystallite size was determined by using Scherrer's formula.

Two-probe resistivity method was used to study the effect of substrate temperature on the electrical property of PdO–NiO–SDC film in the temperature range 27–300 °C. The method has been reported in detail in our previous work [33].

Scanning electron microscope (SEM) images of the films were taken by using scanning electron microscope model JEOL JSM 6360. Composition of the deposited film was determined by energy dispersive X-ray analysis technique (EDAX), using JEOL JSM 6360 SEM model. Grain size and surface roughness of the film were measured by using atomic force microscope (AFM) model, nanoscope E of Digital Instruments, USA in contact mode, with V-shape silicon nitride cantilever of length 100 μm and spring constant 0.58 N/m.

Two-probe impedance measurement technique was used for impedance measurement. Two contacts were drawn on PdO–NiO–SDC spray deposited film with silver paste. Impedance measurement of the film was carried out in air at 350 °C using LCR meter bridge (model HP 4284A) with frequency range of 100 Hz to 1 MHz and amplitude of 1 V. In this technique a brass block was used as sample holder cum heater. The area of the film on the glass substrate was defined as 1.1 cm × 1.1 cm and silver paste was applied to ensure the ohmic contact to the film. Two press contacts were made to the film with the help of pointed brass screws. Cromel–Alumel thermocouple was used to measure the temperature.

3. Results and discussion

3.1. DTA–TGA

Thermal events corresponding to the crystallization process of the deposited material were identified in thermal analysis. Fig. 1 shows the DTA–TGA curves of the PdO–NiO–SDC powder scratched from the PdO–NiO–SDC film deposited at substrate temperature 350 °C on the glass substrate.

A weak exothermic peak at about 250 °C has been observed in DTA curve. TGA curve shows weight loss of 1.354% in between the temperature 225 and 350 °C. This weight loss corresponds to the removal of remains of nitrate precursor solution form deposited material by its thermal decomposition. In both TGA and DTA curves, no remarkable change was detected after 350 °C, indicating that decomposition temperature of the precursor solution is at about 350 °C.

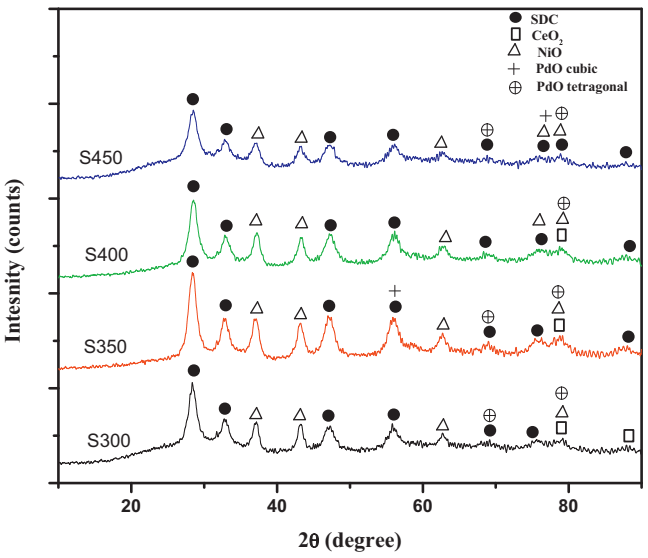

Fig. 2. XRD Patterns of S300, S350, S400 and S450 PdO–NiO–SDC films.

From this study it can be concluded that, in order to have complete phase formation there is necessity to post heat treat the as deposited films. The post heat treatment may help to remove the residue present in the film. The substrates used were of glass and glass starts to melt above 500–550 °C. Hence, in the present investigation, films were post heat treated at 500 °C for 2 h in tube furnace.

3.2. Effect of substrate temperature on the XRD patterns of the PdO–NiO–SDC films

The phase evolution of the PdO–NiO–SDC films deposited at substrate temperatures 300, 350, 400 and 450 °C by spray pyrolysis technique and further heat treated at 500 °C was examined by X-ray diffraction technique and has been shown in Fig. 2. XRD patterns of films show peaks confirming their poly-crystalline nature. In case of SDC based materials, it is reported earlier that, as deposited SDC material is found to be amorphous in nature and crystallization of it occurred by calcining it at 600 °C [34] or 400 °C [35]. But in the present work as deposited films are also found to be well crystalline in nature.

All peaks have been identified and indexed from the known patterns of the standard data files [CeO_2 (cubic) – JCPDS Card No. 34-394, SDC (cubic) – JCPDS Card No. 75-0158, PdO cubic – JCPDS Card No. 46-1211, PdO tetragonal – JCPDS Card No. 43-1024].

Film consists of separate peaks corresponding to, NiO, SDC, and PdO phases, showing the formation of composite films. No reaction was observed between these phases. Lattice constant '*a*' have been calculated and are found to well matched with the standard '*a*' values of 5.433 Å, 4.177 Å, 5.637 Å and 3.043 Å, of cubic SDC, cubic NiO, cubic PdO and tetragonal PdO phases respectively as listed in Table 1. Also, lattice parameter values for SDC phases matches well with the earlier reported values [33,36,37].

The lattice constants of ceria and SDC were reported as 0.5411 nm and 0.5433 nm respectively [38]. From Table 1, if lattice constant value corresponding to SDC cubic phase are compared to ceria phase (a = 5.4113 Å), an increase in '*a*' value has been observed. This increase in '*a*' value is due to the substitution of Sm^{3+} at Ce^{3+} site. Additionally, the effective ionic radius of samarium (0.1219 nm) is higher than that of cerium (0.1110 nm) these combined factors give rise to increase in lattice parameter.

At the substrate temperatures 300, 350 and 400 °C, the calculated cell parameters for few SDC phases are found to be smaller than the theoretical value of $Ce_{0.8}Sm_{0.2}O_{1.9}$ showing little samarium incorporating into the ceria lattice.

From Table 1, it is clear that the lattice constant values increases with pyrolysing temperature, which suggests that samarium ions were dissolved into ceria at higher temperatures. The lattice constant of S450 film is almost same that of SDC cubic phase. Thus, in the present work, samarium ions were dissolved into ceria at or less than 450 °C and this temperature is less than that of reported by others [34,35], this might be due to the better solubility of Sm_2O_3 in CeO_2 lattice. From Fig. 2 it is observed that, (1 1 1) reflection, lying at about $2\theta = 28°$, corresponding to cubic fluorite SDC phase and (1 1 1) reflection lying at about $2\theta = 37°$ corresponding to cubic NiO phase are most intense one. Analyzing these peaks crystallite size of the deposited film was calculated by using Scherrer's formula [39] and is summarized in Table 2.

$$d = \frac{0.9\lambda}{\beta \cos\theta} \quad (2)$$

where d = crystallite size of the material, λ = wavelength of the X-ray radiation, β = full width at half maxima and θ = angle of diffraction.

Table 1
Comparison of '*d*' values and lattice constants of S300, S350, S400 and S450 PdO–NiO–SDC films.

h k l	*d* std (Å)	*a* std (Å)	S300		S350		S400		S450		Crystal structure
			d (cal) (Å)	*a* (cal) (Å)	*d* (cal) (Å)	*a* (cal) (Å)	*d* (cal) (Å)	*a* (cal) (Å)	*d* (cal) (Å)	*a* (cal) (Å)	
1 1 1	3.1367	5.4330	3.1443	5.4462	3.1389	5.4368	3.1262	5.4148	3.1316	5.4241	SDC cubic
0 0 2	2.7165	5.4330	2.7143	5.4286	2.7268	5.4537	2.7264	5.4528	2.7268	5.4537	SDC cubic
0 2 2	1.9208	5.4330	1.9217	5.4354	1.9159	5.4191	1.9140	5.4137	1.9217	5.4354	SDC cubic
1 1 3	1.6381	5.4330	–	–	1.6358	5.4253	1.6371	5.4298	1.6371	5.4298	SDC cubic
0 0 4	1.3582	5.4330	1.3570	5.4282	1.3596	5.4385	1.3657	5.4629	1.3570	5.4282	SDC cubic
1 3 3	1.2464	5.4330	1.2520	5.4575	1.2471	5.4362	1.2478	5.4392	1.2506	5.4514	SDC cubic
2 2 4	1.1090	5.4330	–	–	1.1081	5.4290	1.1091	5.4338	1.1102	5.4388	SDC cubic
0 2 4	1.2148	5.4330	–	–	–	–	–	–	1.2123	5.4217	SDC cubic
4 2 0	1.2100	5.4113	1.2085	5.4040	1.2091	5.4074	1.2097	5.4103	–	–	CeO_2 cubic
4 2 2	1.1046	5.4113	1.1046	5.4118	–	–	–	–	–	–	CeO_2 cubic
1 1 1	2.4115	4.1770	2.4160	4.1846	2.4191	4.1901	2.4097	4.1738	2.4128	4.1792	NiO cubic
2 0 0	2.0885	4.1770	2.0901	4.1803	2.0901	4.1802	2.0809	4.1619	2.0855	4.1711	NiO cubic
2 2 0	1.4767	4.1770	1.4805	4.1875	1.4805	4.1875	1.4731	4.1666	1.4752	4.1726	NiO cubic
3 1 1	1.2594	4.1770	–	–	–	–	–	–	1.2558	4.1653	NiO cubic
2 2 2	1.2057	4.1770	1.2085	4.1863	1.2091	4.1885	1.2097	4.1908	1.2123	4.1997	NiO cubic
2 2 2	1.6000	5.6370	–	–	1.6358	5.6666	–	–	–	–	PdO cubic
4 2 0	1.260	5.6370	–	–	–	–	–	–	1.2558	5.6165	PdO cubic
2 1 0	1.3609	3.0430	1.3570	3.0344	1.3596	3.0402	–	–	1.3570	3.0344	PdO tetragonal
2 1 2	1.2123	3.0430	1.2085	3.0300	1.2091	3.0331	1.2097	3.0349	1.2123	3.0115	PdO tetragonal

Table 2
Crystallite size corresponding to (1 1 1) CeO_2 and NiO peaks in S300, S350, S400 and S450 PdO–NiO–SDC films.

PdO–NiO–SDC films	Crystallite size of NiO (nm)	Crystallite size of SDC (nm)
S300	10.59	8.60
S350	14.23	7.84
S400	9.93	8.18
S450	9.37	8.44

From Table 2, it can be seen that crystallite size of NiO phases is in the range of 9–14 nm and for SDC phases is 7–9 nm. Thus, NiO is most likely to be coarse due to the low melting point of Ni as compared to SDC, similar observations were reported by Yoshida et al. [38].

3.3. Morphological studies

3.3.1. SEM studies

Two dimensional surface morphology of PdO–NiO–SDC films was studied by using scanning electron microscope. Fig. 3 shows SEM images of (a) S300 (b) S400 and (c) S450 PdO–NiO–SDC films. Films show good microstructure with sufficient porosity. Good connectivity between the deposited material has been observed. S300, and S400 films were crack free but few cracks have been observed in S450 films. This may be due to the cracking of the film at the time of post heating. Large shining cubic crystallites were observed on the film surface and these are might be due to deposition of Pd on the film surface. Such type of appearance of the doped noble metal has been reported earlier in the case of rhodium and ruthenium doped samples [40]. Fig. 4 shows SEM images of S350 PdO–NiO–SDC film at different magnifications (a) 1000× (b) 2000× and (c) 5000×.

From Figs. 3 and 4 it is clear that S350 film is crack free and having larger pores along with the few pin holes in it, thus providing sufficient gas flow channels. Good connectivity between the different deposited phases has been observed. Thus the S350 film has good microstructure suitable for its application as SOFC anode material as compared to other films. The present microstructure of the film may help to extend the reaction site from the three phase boundaries to the surface of mixed ionic conductor electrode. Thus, the suitable anode microstructure was fabricated by the spray pyrolysis technique.

3.3.2. AFM studies

AFM images of S350 PdO–NiO–SDC film were taken to determine the grain size and the surface roughness of the film. Fig. 5(a) and (c) shows two dimensional and Fig. 5(b) and (d) shows three dimensional AFM images of the film respectively at two different locations. From Fig. 5 it is clear that, film is made up of nano-sized spherical grains. All phases are found to be well distributed through out the film. Good connectivity of the deposited material was observed. Pores of size 1–2 μm were observed on the film surface. These pores may be helpful for the continuous supply of fuel during operation. This microstructure of the film may help to increase the length of three phase boundary. Surface roughness of the film was calculated with a statistical parameter-root mean square (rms or R_q).

$$R_q = \sqrt{\frac{\sum_{i=1}^{N}(Z_i - Z_{avg})^2}{N}} \quad (3)$$

where Z_{avg} is the average of Z values within given area, Z_i is the current and N is the number of points within given area. Particle size was found to be 70 nm. The particle size observed in AFM analysis is somewhat larger than that calculated from XRD analysis. This indicates that the crystallites are little bit agglomerated to form larger particle. Surface roughness of the film was found to be 5.2 nm indicating smooth surface morphology.

3.4. Compositional study

The composition of the deposited film was determined by using energy dispersive X-ray analysis technique. Fig. 6 shows EDAX pattern of S350 PdO–NiO–SDC thin film.

It shows peaks corresponding to the elements Ce, Sm, O, along with the elemental peaks corresponding to Ni and Pd, thus show-

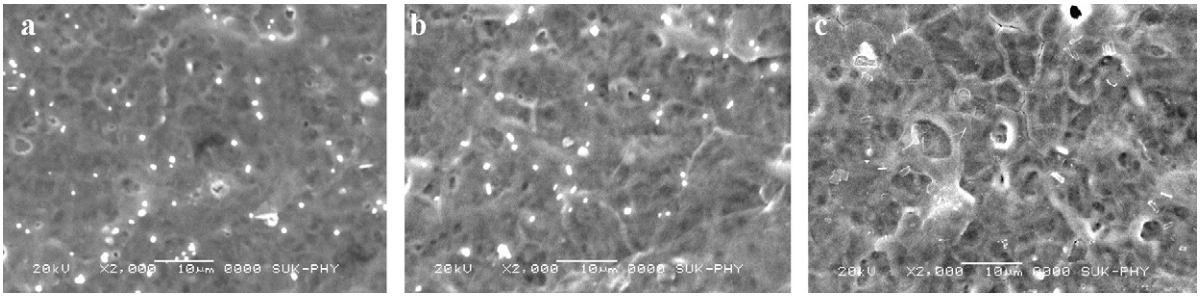

Fig. 3. SEM images of (a) S300 (b) S400 and (c) S450 PdO–NiO–SDC films.

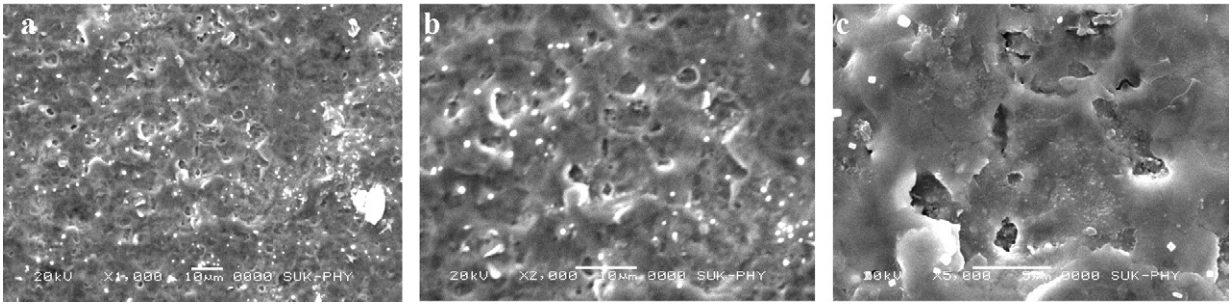

Fig. 4. SEM images of S350 PdO–NiO–SDC films at different magnifications (a) 1000× (b) 2000× and (c) 5000×.

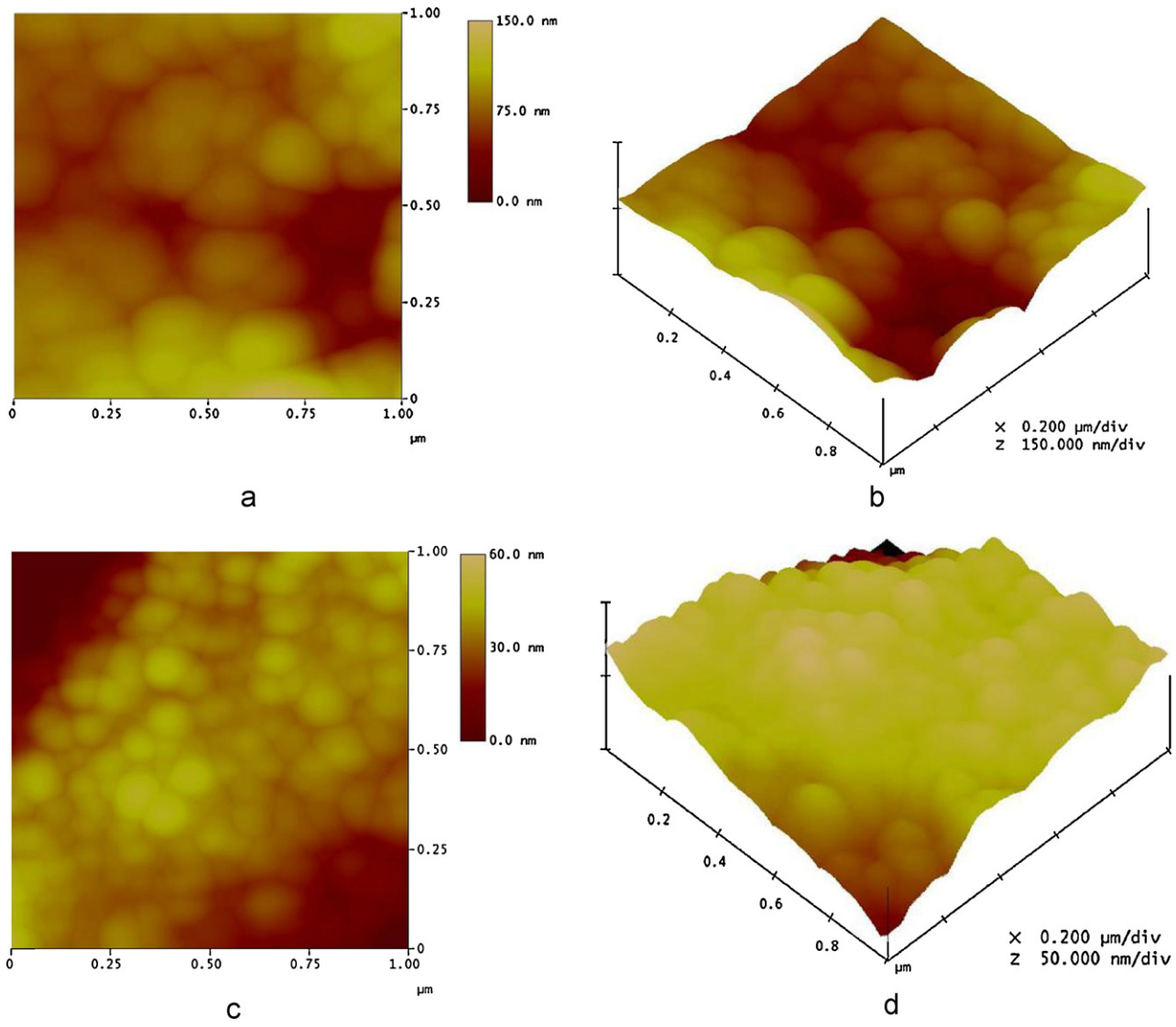

Fig. 5. AFM images of S350 PdO–NiO–SDC thin film at different locations (a and c) two dimensional and (b and d) three dimensional.

ing the formation of film with desired elements. No other impurity peaks were observed.

3.5. Effect of substrate temperature on DC electrical resistivity of PdO–NiO–SDC film

Two-probe resistivity method was used to study the electrical property of S300, S350, S400 and S450 PdO–NiO–SDC films. The method is described in detail elsewhere [33]. Resistivity of the film was studied in the temperature range 27–300 °C. Fig. 7 shows plot of log ρ vs. $1/T$ of S300, S350, S400, and S450 PdO–NiO–SDC films.

From Fig. 7 it can be seen that the resistivity of all the films decreases with increase in the temperature showing semiconducting nature. Fig. 7 shows that, the resistivity of S450 film is higher than that of other films; this is due to the presence of cracks in the film, as observed in Fig. 3. Among these films S400 film shows higher conductivity compared to other films. From Figs. 3 and 4 it is clear that the S400 film is less porous as compared to S350 film. It is reported that, the anodes of SOFCs should have high electronic conductivity, adequate porosity for gas transport and high oxygen ion conductivity [41]. Hence from XRD, SEM, AFM and resistivity studies S350 film has been selected for further study. DC resistivity of the film was found to be 10^1 Ω cm at 300 °C. Activation energies of the deposited film were calculated by using the relation [42].

$$\rho = \rho^0 \exp\left(\frac{E_a}{kT}\right) \quad (4)$$

where ρ is the resistivity, E_a is the activation energy, k is the Boltzmann's constant and T is the absolute temperature. Activation energy was found to be 0.24 eV which is comparable to the earlier reported values for NiO–SDC [20] and lower than that reported for doped ceria [33,43,36].

3.6. Complex impedance measurements of PdO–NiO–SDC film

The method of complex impedance analysis [44] has emerged as very powerful tool for separating out contributions due to intragrain, grain boundary and electrode processes. Using HP4284A LCR-Q meter, the measurement of resistance (R) and reactance (X) were carried out at the temperature 350 °C. Fig. 8 shows nyquist plot at 350 °C of spray deposited S350 PdO–NiO–SDC film. The frequency was varied from 100 Hz to 1 MHz. Silver paste was used to draw the electrical contacts on the film. Electrode area was selected as 1.1 cm × 1.1 cm. At this temperature in higher frequency range above 1 kHz, the impedance response was characterized by a very large single semi circle; this semicircle in higher frequency range

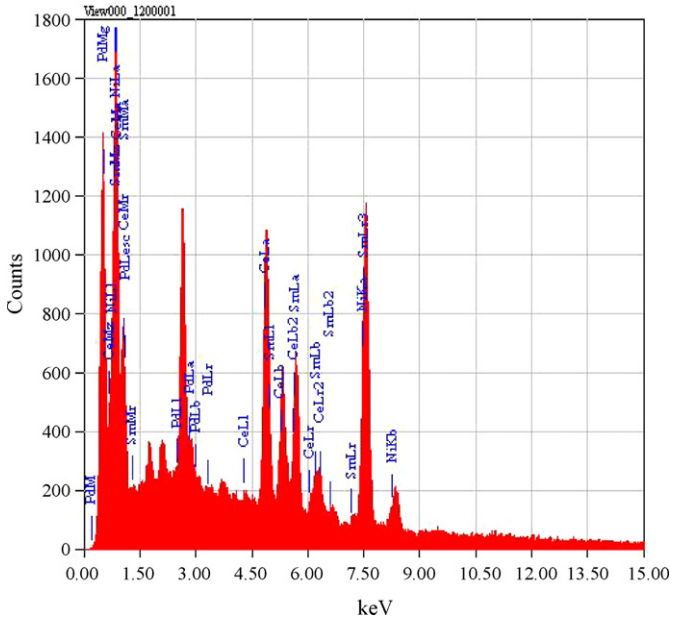

Fig. 6. EDAX pattern of spray deposited PdO–NiO–SDC film.

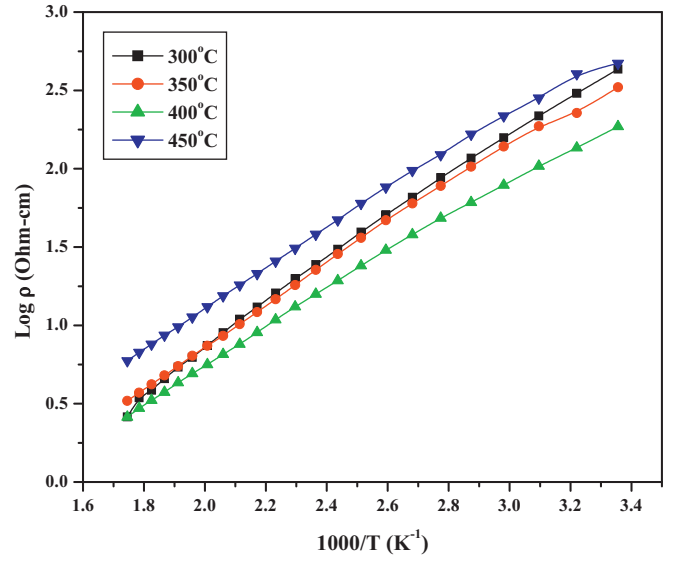

Fig. 7. Plot of log ρ vs. $1/T$ of S300, S350, S400, and S450 PdO–NiO–SDC films.

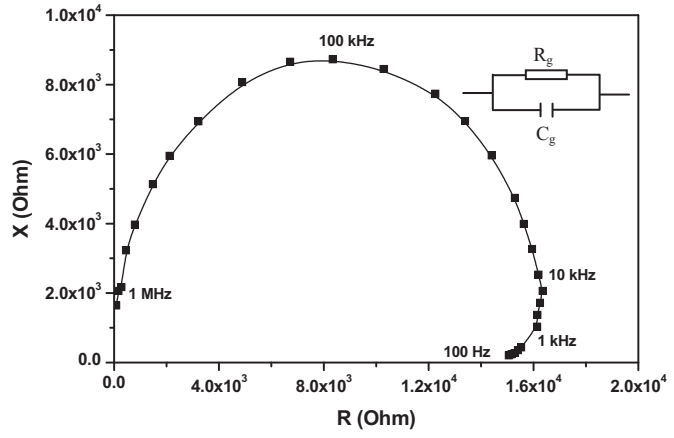

Fig. 8. Nyquist plot at 350 °C for spray deposited S350 PdO–NiO–SDC film.

corresponds to the oxygen ion migration in the bulk [45]. It has been modelled to an equivalent circuit comprising of combination of bulk resistance (R_g) and bulk capacitance (C_g) as shown in inset of Fig. 8.

From Fig. 8 it has been also seen that the bulk resistance of the material at 350 °C is $1.49 \times 10^4\ \Omega$. A.C. conductivity of the film at 350 °C temperature was calculated by using equation

$$\sigma_{ac} = \frac{d}{RA} \quad (5)$$

where σ_{ac} is the conductivity $(\Omega\,\mathrm{cm})^{-1}$, R is the resistance measured (Ω), d is the distance between voltage electrodes (cm) and A is the cross sectional area of the electrode (cm^2). A.C. conductivity is found to be 3.9×10^{-1} $(\Omega\,\mathrm{cm})^{-1}$ at 350 °C. The conductivity value is higher than that reported by others for doped ceria anodes [20,43].

It has been reported that a microcrystalline material fares far better in terms of ionic conductivity than that the nano-crystalline material [46]. It has been also reported that, the grain boundary resistivity changes with the grain size. When the grain size decreases from a few micrometers to the nano level, the grain boundaries show unusually high conductivity [47–49]. This may be due to the fact that, in nano-crystalline materials grain boundaries have high defect densities and the atoms there have high mobility and these are the two important factors for increase in the ionic conductivity. Hence, the ionic conductivity may be significantly enhanced in nano-crystalline materials compared to the microcrystalline ones [47,50], and same has been observed in the present work.

3.7. Consideration of PdO–NiO–SDC material as IT-SOFC anode

Recently, the influence of palladium addition to the NiO–SDC or NiO–GDC anodes on the cell performance has been studied and compared to an unmodified cell. It has been reported that Pd containing anode allow for higher power outputs [26–28]. This is due to the fact that metals (Pd, Pt, Rh) had much higher specific rates for water gas shift, steam reforming and carbon dioxide reforming of methane when supported on ceria than when supported on silica or alumina [29,30]. Pd, Pt, and Ru show far higher oxidation activity than ceria or any other oxide [31]. Thus, an addition of an oxidation catalyst such as Pd can promote complete oxidation of hydrocarbon and generate more heat to increase the cell temperature [26].

Since precious metals such as Pt, Pd and Rh show high catalytic activity towards breaking the C–H bond of CH_4 [51–54]. CH_4 would firstly be catalyzed to form C and H_2 when these electro-catalysts are dispersed on the surface of anode [55]. Subsequently, H_2 produced by the CH_4 decomposition, electrochemically oxidized to H_2O. Then produced H_2O reacts with the deposited carbon and produces CO and H_2. Secondarily produced CO and H_2 are electrochemically oxidized to CO_2 and H_2O again. Thus the surface of the anode can be kept clean during cell operation. This methane oxidation mechanism is proposed by Zhu et al. [56] for Pd-impregnated anode, and the similar mechanism may be present in the spray deposited PdO–NiO–SDC anode material.

Thus, the presence of ceria/samaria doped ceria may improve the properties of anode material regarding its sensitivity to deactivation by carbon deposition [57–59]. The presence of samaria doped ceria and palladium may improve the sulfur tolerance of the anode material [14–17,60]. Also as compared to the conventional SOFC anode materials, high oxide conduction in doped ceria anode can make it possible to decrease the SOFC operating temperature down to 600–800 °C. As a result of this the cost of SOFC technology may be dramatically reduced since much less expensive materials can be used in cell construction and novel fabrication techniques can be applied to the stack and system integration. As

the operating temperature is reduced, system reliability and operational life may increase. From the above discussion it is clear that, the spray deposited PdO–NiO–SDC material has been found to fulfill the requirements of the intermediate temperature SOFC anode material and hence can be considered as a potential anode material for its application in IT-SOFCs.

4. Conclusions

Nano-crystalline, adherent, porous, PdO–NiO–SDC composite thin films have been successfully deposited by a simple and cost effective spray pyrolysis technique for the first time. All films were found to be well crystalline in nature and showing separate peaks corresponding to NiO, SDC and PdO phases. Films show good microstructure with sufficient porosity and good connectivity of the deposited material. Crystallite size of the deposited material was found to be in the range of 7–9 nm. The deposited film showed high oxygen ion conductivity, 3.94×10^{-1} S cm^{-1} at 350 °C. As anode is composed of smaller SDC and Ni particles, hence during operation, electrochemical reaction area can be larger and anodic polarization can be smaller than that of conventional SOFC anode.

Acknowledgements

One of the authors, B.B.P is thankful to the Ministry of New and Renewable Energy (MNRE), New Delhi for providing financial assistance. They are also indebted to U.G.C. and C.S.I.R., Delhi for their financial support. Author B.B.P is also thankful to Mr. Rahul Mulik and Ms. Siddhi Mulik for their kind support.

References

[1] N.Q. Minh, J. Am. Ceram. Soc. 76 (1993) 563.
[2] W. Sun, X. Huang, Z. Lu, L. Zhao, B. Wei, S. Li, K. Chen, N. Ai, W. Su, J. Phys. Chem. Solids 70 (2009) 164.
[3] J.R Rostrup-Nielson, Catalytic Steam Reforming, Springer Verlag, Berlin, 1984.
[4] M.L. Toebes, J.H. Bitter, A.J. van Dillen, K.P. de Jong, Catal. Today 76 (2002) 33.
[5] D. Simwonis, F. Tietz, D. Stover, Solid State Ionics 132 (2000) 241.
[6] R. Aguiar, F. Sanchez, C. Ferrater, M. Varela, Thin Solid Films 306 (1997) 74.
[7] A. Trovarelli, C. de Leitenburg, M. Boaro, G. Dolcetti, Catal. Today 50 (1999) 353.
[8] B.C.H. Steele, P.H. Middleton, R. Rudkin, Solid State Ionics 40/41 (1990) 388.
[9] I.S. Metcalfe, P.H. Middleton, P. Petrolekas, B.C.H. Steele, Solid State Ionics 57 (1992) 259.
[10] M. Gong, X. Liu, J. Trembly, C. Johnson, J. Power Sources 168 (2007) 289.
[11] M. Flytzani-stephanopoulos, M. Sakbodin, Z. Wang, Science 312 (2006) 1508.
[12] H. Devianto, S.P. Yoon, S.W. Nam, J. Han, T.H. Lim, J. Power Sources 159 (2) (2006) 1147.
[13] H. Inaba, H. Tagawa, Solid State Ionics 83 (1–2) (1996) 1.
[14] J.P. Trembly, A.I. Marquez, T.R. Ohrn, D.J. Bayless, J. Power Sources 158 (2006) 263.
[15] P.V. Aravind, J.P. Ouweltjes, E. de Heer, N. Woudstra, G. Rietveld, Proceedings of the 9th International Symposium on Solid Oxide Fuel Cells, 2005, p. 15.
[16] K. Eguchi, J. Alloys Compd. 25 (1997) 486.
[17] G.B. Balazs, R.S. Glass, Solid State Ionics 76 (1995) 155.
[18] X. Huang, Z. Lu, L. Pei, Z. Liu, Y. Liu, R. Zhu, J. Miao, Z. Zhang, W. Su, J. Alloys Compd. 360 (2003) 294.
[19] T Misono, K. Murata, T. Fukui, J. Chaichanawong, K. Sato, H. Abe, M. Naito, J. Power Sources 157 (2006) 754.
[20] B.B. Patil, V. Ganesan, S.H. Pawar, J. Alloys Compd. 460 (2008) 680.
[21] Q. Liu, X. Dong, Yang.F C., S. Ma, F. Chen, J. Power Sources 195 (2010) 1543.
[22] M. Kawano, H. Yoshida, K. Hashino, H. Ijichi, S. Suda, K. Kawahara, T. Inagaki, J. Power Sources 173 (2007) 45.
[23] L. Zhao, X. Huang, R. Zhu, Z. Lu, W. Sun, Y. Zhang, X. Ge, Z. Liu, W. Su, J. Phys. Chem. Solids 69 (2008) 2019.
[24] I. Yamanaka, K. Otsuka, J. Mol. Catal. A 95 (1995) 115.
[25] B.C.H. Steele, Solid State Ionics 129 (2000) 95.
[26] A. Tomita, D. Hivabayashi, T. Hibino, M. Nagao, M. Sano, Electrochem. Solid-State Lett. 8 (2005) A63.
[27] T. Hibino, A. Hashimoto, S. Yoshida, M. Sano, J. Electrochem. Soc. 149 (2002) A133.
[28] Z. Shao, C. Kwak, S.M. Haile, Solid State Ionics 175 (1–4) (2004) 39.
[29] T. Bunluesin, R.J. Gorte, G.W. Graham, Appl. Catal. B 15 (1998) 107.
[30] S. Sharma, S. Hilaire, J.M. Vohs, R.J. Gorte, H.W. Jen, J. Catal. 190 (2000) 199.
[31] S. Putna, J. Stubenrauch, J.M. Vohs, R.J. Gorte, Langmuir 11 (1995) 4832.
[32] H. Inaba, H. Tagawa, Solid State Ionics 83 (1996) 1.
[33] B.B. Patil, S.H. Pawar, Appl. Surf. Sci. 253 (2007) 4994.
[34] J.L.M. Rupp, A. Infortuna, L.J. Gauckler, Acta Mater. 54 (2006) 1721.
[35] J.G. Li, T. Ikegami, T. Mori, Acta Mater. 52 (2004) 2221.
[36] J. Ma, C. Jiang, X. Zhou, G. Meng, X. Liu, J. Alloys Compd. 455 (2008) 364.
[37] T. Karaca, T.G. Altincekic, M.F. Oksuzomer, Ceram. Int. 36 (2010) 1101.
[38] H. Yoshida, H. Deguchi, M. Kawano, K. Hashino, T. Inagaki, H. Ijichi, M. Horiuchi, K. Kawahara, S. Suda, Solid State Ionics 178 (2007) 399.
[39] H.P. Klug, L.E. Alexander, X-ray Diffraction Procedure for Polycrystalline and Amorphous Material, Wiley, New York, 1954, p. 491.
[40] U. Hennings, R. Reimert, Appl. Catal. B-Environ. 70 (2007) 498.
[41] J.H. Lee, J.W. Heo, D.S. Lee, J. Kim, G.H. Kim, H.W. Lee, H.S. Song, J.H. Moon, Solid State Ionics 158 (2003) 225.
[42] R. Kassing, W. Bax, Jpn. J. Appl. Phys. Suppl. 2 (Pt. 1) (1974) 801.
[43] G. Ruifeng, M. Zongqiang, J. Rare Earth 25 (2007) 364.
[44] A. Hopper, J. Phys. D: Appl. Phys. 10 (1976) 1487.
[45] S. Sameshima, H. Ono, K. Higashi, K. Sonoda, Y. Hirata, Y. Ikuma, J. Ceram. Soc. Jpn. 108 (12) (2000) 1058.
[46] J.L.M. Rupp, A. Infortuna, L.J. Gauckler, J. Am. Ceram. Soc. 90 (6) (2007) 1792.
[47] H.L. Tuller, Solid State Ionics 131 (2000) 143.
[48] R. Gerhardt, A.S. Nowick, J. Am. Ceram. Soc. 69 (1986) 641.
[49] Y.M. Chiang, E.B. Lavik, I. Kosacki, H.L. Tuller, J.Y. Ying, Appl. Phys. Lett. 69 (1996) 186.
[50] B.B. Patil, S.H. Pawar, J. Alloys Compd. 509 (2) (2011) 414.
[51] S. McIntosh, J.M. Vohs, R.J. Gorte, Electrochem. Solid-State Lett. 6 (2003) A240.
[52] H. Uchida, N. Mochizuki, M. Watanabe, J. Electrochem. Soc. 143 (1996) 1700.
[53] M. Watanabe, H. Uchida, M. Shibata, N. Mochizuki, K. Amikura, J. Electrochem. Soc. 141 (1994) 342.
[54] H. Uchida, S. Suzuki, M. Watanabe, J. Electrochem. Solid-State Lett. 6 (2003) A174.
[55] Y. Nabae, I. Yamanaka, M. Hatano, K. Otsuka, J. Electrochem. Soc. 151 (2006) A140.
[56] X.C. Lu, J.H. Zhu, Solid State Ionics 178 (2007) 1467.
[57] H. Roh, K. Jun, W. Dong, S. Park, Y. Baek, Catal. Lett. 74 (2001) 31.
[58] H. Roh, H. Potdar, K. Jun, J. Kim, Y. Oh, Appl. Catal. A-Gen. 276 (2004) 231.
[59] F. Passos, E. de Oliveira, L. Mattos, F. Noronha, Catal. Today 101 (2005) 23.
[60] R. Ahlborn, F. Baumann, S. Wieland, EP 1 157 968 (2001), Hanau, Germany.